Journal of Photochemistry and Photobiology A: Chemistry 206 (2009) 177–187

Contents lists available at ScienceDirect

Journal of Photochemistry and Photobiology A: Chemistry

journal homepage: www.elsevier.com/locate/jphotochem

Photoactivity of mechanochemically prepared nanoparticulate titanium dioxide investigated by EPR spectroscopy

Vlasta Brezová[a,*], Zuzana Vrecková[a], Peter Billik[b], Mária Čaplovičová[b], Gustav Plesch[b]

[a] Institute of Physical Chemistry and Chemical Physics, Faculty of Chemical and Food Technology, Slovak University of Technology in Bratislava, Radlinského 9, SK-812 37 Bratislava, Slovak Republic

[b] Faculty of Natural Sciences, Comenius University, Mlynská dolina, Bratislava, SK-842 15, Slovak Republic

ARTICLE INFO

Article history:
Received 3 March 2009
Received in revised form 22 June 2009
Accepted 28 June 2009
Available online 9 July 2009

Dedicated to Professor Andrej Staško on the occasion of his 70th birthday.

Keywords:
Titanium dioxide
Mechanochemical synthesis
EPR spectroscopy
Spin trapping
Absorption and scattering

ABSTRACT

Titanium dioxide nanopowders were prepared by mechanochemical synthesis in a high-energy ball mill using $TiOSO_4 \cdot xH_2O$ and Na_2CO_3 followed by annealing in the temperature range 200–800 °C. The UVA photonic efficiency of radical processes on synthesized TiO_2 powders was determined by *in situ* EPR spectroscopy, using, as indicators, the *N*-oxide spin trapping agents (5,5-dimethyl-1-pyrroline *N*-oxide and 5-(diisopropoxy-phosphoryl)-5-methyl-1-pyrroline *N*-oxide) or the radical cation of 2,2′-azino-bis(3-ethylbenzothiazoline-6-sulfonate, $ABTS^{\bullet+}$). The results obtained by monitoring the photoinduced generation of hydroxyl radical spin adducts correlated with those found by the investigation of the photoreduction of $ABTS^{\bullet+}$. The presence of iron and chromium ions, which were evidenced in samples milled in steel, decreased the photonic efficiency of radical processes. The presence of a sulfate salt matrix during the annealing process distinctly inhibits the transformation of anatase to rutile. The highest photocatalytic activity was shown by anatase samples which were prepared by milling in corundum and annealed at 700 °C. They were composed of crystallites with a mean size of 25–30 nm and well developed crystal faces.

1. Introduction

The photoinduced heterogeneous processes on titanium dioxide surfaces attract substantial attention of multidisciplinary research due to their potential large-scale applications in the remediation of polluted water, soil and air [1–3], in unconventional organic synthesis [4–6], and in the preparation of self-cleaning surfaces [7–9]. The character and surface properties of titania nanocrystals strongly influence the physico-chemical behaviour of synthesized materials upon irradiation [10–12]. Electron paramagnetic resonance (EPR) spectroscopy is a valuable tool for monitoring the radical-producing capacity of TiO_2 upon UVA irradiation as well for the study of paramagnetic transition metal ions within the titania matrix [13–15]. Recently, the effect of size and shape of nanocrystalline TiO_2 on photogenerated charges was investigated by EPR spectroscopy at temperatures below 80 K, evidencing the formation of paramagnetic species assigned to electrons (e^-) trapped at lattice titanium within the bulk ($Ti(III)_{latt}$) and holes (h^+) trapped at oxygen atoms on the nanocrystal surface [16]. Detailed analysis of the EPR spectra of charge carriers generated upon UV exposure of mixed-phase TiO_2 at 10 K (holes trapped at O^- lattice; electrons trapped at Ti(III) and O_2^-) revealed correlation between TiO_2 particle size/shape and photoactivity [17]. EPR investigations of super-oxide radical anions on titanium dioxide P25 (Aeroxide®, Evonik Degussa, Germany) confirmed their stabilization specifically at anion vacancy sites, and these stabilized radicals possess higher chemical and photochemical reactivity comparing to surface super-oxide radicals bound at non-vacancy sites [18]. In oxygenated aqueous media the irradiation of TiO_2 particles at room temperature resulted in the generation of short-lived reactive oxygen species ($^\bullet OH$, $^\bullet OOH/O_2^{\bullet-}$, $^1O_2$) [19–23]. The photo-produced reactive radical intermediates may be studied by cw-EPR spectroscopy using the spin trapping agents (DMPO, DIPPMPO, POBN) or by the termination of semi-stable free radicals added into photoactive heterogeneous TiO_2 systems (TEMPOL, DPPH, $ABTS^{\bullet+}$) [19–24].

The mechanochemical synthesis, using high-energy ball milling with subsequent thermal activation, is a promising way for producing photoactive titanium dioxide nanopowders, where modifications of the chemical precursors, alterations of the milling

Abbreviations: ABTS, 2,2′-azino-bis(3-ethylbenzothiazoline-6-sulfonate) diammonium salt; DIPPMPO, 5-(diisopropoxy-phosphoryl)-5-methyl-1-pyrroline *N*-oxide; DMPO, 5,5-dimethyl-1-pyrroline *N*-oxide; DPPH, 1,1-diphenyl-2-picrylhydrazyl; EDX, energy dispersive X-ray spectroscopy; E_{bg}, band-gap energy; EPR, electron paramagnetic resonance; POBN, α-(4-pyridyl-1-oxide)-*N*-*tert*-butylnitrone; SW, magnetic field sweep width; TEMPOL, 4-hydroxy-2,2,6,6-tetramethylpiperidine *N*-oxyl; UV/vis, ultraviolet/visible; XRD, X-ray diffraction; TEM, transmission electron microscopy.

* Corresponding author. Tel.: +421 2 5932 5666; fax: +421 2 5292 6032.
E-mail address: vlasta.brezova@stuba.sk (V. Brezová).

1010-6030/$ – see front matter © 2009 Elsevier B.V. All rights reserved.
doi:10.1016/j.jphotochem.2009.06.006

conditions, the presence of salt matrices and variations in the annealing temperature permit the preparation of titania nanomaterials with the required structure and particle size [25–30]. Until recently only preliminary studies of their photocatalytic activity have been reported [25,26].

Our investigation is focused on the characterization of the structure, optical properties and photoactivity of titania nanopowders mechanochemically synthesized under different experimental conditions.

2. Experimental

2.1. Chemicals and reagents

Titanium dioxide powder samples were prepared by mechanochemical synthesis using $TiOSO_4 \cdot xH_2O$ (Riedel de Haen) and Na_2CO_3 (Lachema, Czech Republic) as starting reactants. The reaction was performed in a high-energy ball mill using stainless steel (series SSM, steel salt matrix, and S, steel) or corundum jars (series CSM, corundum salt matrix), respectively [26,27]. The final products in series SSM and CSM were obtained by annealing the milled powders in the temperature range 200–800 °C and subsequent washing out of the water-soluble byproduct $Na_2SO_4 \cdot xH_2O$. The annealing process of powders synthesized in series S was performed without a salt matrix, which was washed out immediately after milling. A summary of the samples investigated is given in Table 1. The commercial photoactive titanium dioxide Aeroxide® P25 was kindly provided by Evonik Degussa (Germany). The TiO_2 stock suspensions (1×10^{-3} g cm^{-3}) were prepared by sonication in distilled water.

The spin trapping agent, 5,5-dimethyl-1-pyrroline *N*-oxide (DMPO; Aldrich) was distilled before application. 5-(Diisopropoxy-phosphoryl)-5-methyl-1-pyrroline *N*-oxide (DIPPMPO; Alexis® Biochemicals) was used without purification. The concentration of photogenerated adducts was determined using aqueous solutions of 4-hydroxy-2,2,6,6-tetramethylpiperidine *N*-oxyl (TEMPOL; Aldrich) as calibration standards.

Radical cation of 2,2′-azino-bis(3-ethylbenzothiazoline-6-sulfonate) diammonium salt (ABTS; Sigma) was prepared by dissolving 17.2 mg of ABTS and 3.3 mg of $K_2S_2O_8$ (Aldrich) in 5 mL of distilled water as described in Ref. [24]. The prepared solutions of $ABTS^{\bullet+}$ were diluted immediately before measurements, to obtain the optimal concentration for photoinduced EPR and UV/vis experiments (30 μM).

2.2. Methods and apparatus

2.2.1. X-ray powder diffraction and TEM study

The prepared powders were characterized by X-ray powder diffraction using a Philips PW 1050 diffractometer and Cu-Kα radiation. The size of the anatase nanocrystallites was calculated from the full width at half maximum height of the 101 XRD diffraction of anatase according to Scherrer's equation [28]. The anatase/rutile ratio was calculated according to Ref. [31].

Transmission electron microscopy (TEM) was performed on a TEM JEOL 2000FX device working at accelerating voltages of 160 and 200 kV. The powder samples were dispersed using ultrasound. A small amount of powder was mixed with ethanol and subjected to vigorous ultrasound stirring for 10 min. Subsequently a drop of strongly diluted ethanol suspension was deposited onto the TEM Cu-grid, which was previously covered with a holey carbon film. After drying in air the samples were examined by TEM.

2.2.2. EPR measurements of powder titania samples

The homogenized TiO_2 powders (15–30 mg) were placed in precise glass EPR capillaries (50 μL; Magnettech, Germany) to produce samples with identical dimensions (column height 4.6 ± 0.2 cm). The sample was then inserted into a standard TE_{102} (ER 4102 ST) rectangular cavity of an EMX X-band EPR spectrometer (Bruker, Germany) and the EPR spectrum was recorded at 100 or 298 K under air without UVA exposure, consequently no photogenerated paramagnetic species were formed and observed in EPR spectra of titania powders. Temperature control was achieved using a Bruker temperature control unit ER 4111 VT. The concentration of surface-Fe(III) ions in titania powders was calculated from the double integral intensity of the paramagnetic signal characterized by $g_{eff} = 4.3$ using a secondary standard Cr(III) in MgO (99.5 μg Cr(III) in 1 g MgO; Magnettech, Germany). The WIN EPR program (Bruker, Germany) was used for experimental EPR spectra acquisition and manipulation.

2.2.3. UV/vis experiments

UV/visible spectra of titania aqueous suspensions in the wavelength interval 240–600 nm were recorded using a UV-3600 UV/vis spectrometer (Shimadzu, Japan) with a large integrating sphere assembly with a transmittance measurement accessory (1 cm square quartz cell). TiO_2 suspensions with low concentrations (1×10^{-5}–1×10^{-4} g cm^{-3}) were used in the UV/vis experiments. The freshly prepared titania suspensions were sonicated for 1 min (Ultrasonic Compact Cleaner TESON 1, Tesla, Slovak Republic), and

Table 1
Phase composition, anatase crystallite size, absorption and scattering coefficient at λ = 365 nm, and band-gap energy of titania powders prepared by milling in various jars and annealed at different temperatures. The samples are designated by a capital letter and a number, characterizing the synthesis series and the annealing temperature.

TiO_2 sample	Annealing temperature (°C)	Phase composition anatase/rutile	Mean crystallite size of anatase (nm)	$\varepsilon^{\lambda}_{abs}$ (cm^2 g^{-1})	$\varepsilon^{\lambda}_{scat}$ (cm^2 g^{-1})	E_{bg} (eV)
S25	25	Amorph.	–	750	7 100	–
S200	200	Amorph.	–	1800	3 700	–
S300	300	Low crystallinity	~2	250	5 600	3.24
S400	400	–	12	1600	5 600	3.25
S500	500	62/38	15	1000	14 000	3.2
S600	600	54/46	28	6000	4 000	3.05
S700	700	51/49	68	2300	13 000	3.06
S800	800	17/83	~140	2000	9 000	3.01
SSM300	300	100/[a]	~2	300	2 600	–
SSM400	400	100/[a]	15	1100	2 400	–
SSM500	500	95/5	17	300	1 400	3.21
SSM600	600	93/7	22	3000	3 300	3.25
CSM300	300	100/0	3	30	2 800	3.26
CSM400	400	100/0	7	400	2 500	3.25
CSM500	500	100/0	15	330	3 600	3.20
CSM600	600	100/0	29	2300	2 100	3.25
CSM700	700	100/0	37	3000	11 000	3.27
P25	–	80/20	23	1400	37 000	3.18

[a] Small admixture of rutile phase detected in powder XRD pattern.

then UV/vis spectra were measured in duplicate. The values of absorption and scattering coefficients at the given wavelengths ($\Delta\lambda$ = 5 nm) were evaluated from the experimental data by a least-squares minimization procedure using the Kubelka-Munk model of diffuse reflectance and transmission in accord with Refs. [32,33].

2.2.4. EPR in situ photochemical experiments

The suspensions of TiO_2 containing spin trapping agents (DMPO and DIPPMPO) or radical cation $ABTS^{\bullet+}$ were prepared immediately before the EPR measurements. The stock TiO_2 suspension was homogenized in an ultrasonic bath for 1 min before the addition of the spin trap and dilution to a final concentration of 5×10^{-4} g cm^{-3}. The suspensions were then carefully mixed by a slight air stream and immediately transferred to a small quartz flat cell (WG 808-Q, Wilmad-LabGlass, USA; optical cell length 0.045 cm) optimized for the TE_{102} cavity. The samples were irradiated at 295 K directly in the EPR resonator, and EPR spectra were recorded *in situ*. As an irradiation source an HPA 400/30S lamp (400 W, Philips) was used, emitting radiation mainly between 300 and 400 nm (λ_{max} = 365 nm). The irradiance of the UVA lamp, 2.65 mW cm^{-2}, within the EPR cavity was determined using a UV Light Meter UV-340, Lutron (Lutron Ltd., UK). A Pyrex glass filter (thickness of 1 mm) was used to eliminate radiation wavelengths below 300 nm. The first spectrum in the time-evolution was measured without radiation, and subsequently, upon continuous irradiation ten spectra were recorded. (Each EPR spectrum represents an accumulation of three scans (DMPO or DIPPMPO) or two scans ($ABTS^{\bullet+}$) measured with a 22 s sweep time.) The concentration of spin-adducts was evaluated from double-integrated EPR spectra using the calibration curve obtained by EPR spectra of TEMPOL.

Typical EPR spectrometer settings in a standard photochemical experiment were: microwave frequency, 9.44 GHz; microwave power, 10.03 mW; center field, 335.6 mT; sweep width, 8–10 mT; gain, 2×10^5–1×10^6; modulation amplitude, 0.1–0.2 mT; scan, 20.97 s; time delay, 1.03 s; time constant, 20.48 or 40.96 ms; number of scans, 3 or 2. The *g*-values were determined with an uncertainty of ±0.0001 by simultaneous measurement of a reference standard containing DPPH. The simulations of EPR spectra were carried out using the WIN EPR and SimFonia standard programs (Bruker), and the fitting of experimental spectra by the simulations were obtained by a least-squares minimization procedure using the Scientist program (MicroMath).

2.2.5. Steady-state photochemical experiments

Photochemical experiments with the radical cation $ABTS^{\bullet+}$ were carried out at room temperature (295 K) under air. The freshly prepared TiO_2 suspensions or solutions containing $ABTS^{\bullet+}$ (initial concentration of 30 μM) were irradiated in a standard quartz UV/vis cell (1 cm) with a focused light beam from an HPA source. The UV/vis spectra were recorded using a large integrating sphere assembly with a transmittance measurement accessory (UV-3600, Shimadzu, Japan), using as a reference an analogous TiO_2 suspension, or distilled water, respectively.

3. Results and discussion

3.1. Synthesis of the nanopowders

All of the samples investigated were prepared by mechanochemical synthesis from $TiOSO_4 \cdot xH_2O$ and Na_2CO_3 according to the previously described procedure [26,27]. After milling in a high-energy planetary mill, amorphous precursors of titania were formed. The nanocrystalline TiO_2 products were formed in an annealing step at temperatures in the range of 300–800 °C. The overall reaction can be described by the following chemical Eq. (1):

$$TiOSO_4 \cdot xH_2O + Na_2CO_3 \rightarrow TiO_2 + Na_2SO_4 \cdot xH_2O + CO_2 \quad (1)$$

In the mechanochemical synthesis the contamination by milling elements plays a highly important role on the properties of the obtained product. We prepared samples by milling in stainless steel jars, using chromium–steel balls (series SSM and S), and by milling in corundum jars with corundum balls (series CSM).

The samples of series S were annealed without a salt matrix (the $Na_2SO_4 \cdot xH_2O$ byproduct was washed out prior to the annealing process). In this case the as-milled sample and the powder annealed at 200 °C are amorphous (Table 1). The fact that in the XRD pattern of the as-milled product the diffractions of $TiOSO_4 \cdot xH_2O$ disappeared and peaks of $Na_2SO_4 \cdot 10\ H_2O$ can be recognized allows us to assume that the as-milled product of mechanochemical reaction contains of amorphous TiO_2 [27]. The most intensive diffraction 101 of anatase is resolved in XRD diffractogram of the sample annealed at 300 °C. It is highly broadened, which indicates that the size of the crystallites is very small. A rise in the annealing temperature leads to an increase of rutile content, and rutile prevails in the powder synthesized at 800 °C. The higher temperatures also induce growth of anatase nanoparticles (Table 1). It is well known that the presence of a salt matrix during the annealing of the precursors allows one to improve control over the characteristics of the products of mechanochemical synthesis [25–27]. Therefore we studied the influence of a sulfate salt matrix on the formation of anatase in reaction (1). The samples in the series SSM were annealed in a Na_2SO_4 salt matrix, since water-soluble sulfate was washed out only after the annealing process. In the samples in the SSM series, which were heated in the range of 300–600 °C, the content of rutile admixture is very small. The presence of the sulfate salt matrix evidently inhibits the rutilization of the sample. This is in accordance with the fact that sulfate ions bound on the surface of nanocrystalline TiO_2 inhibit the transformation of anatase to rutile [34,35]. The increase of the size of anatase nanocrystallites with rising temperature in the range of 300–600 °C has in series SSM is similar in character as in series S (Table 1).

In order to avoid the contamination of synthesized nanopowders with transition metals from milling tools, which can act detrimentally on photoinduced activity as centers for charge recombination [26], we prepared a series of samples by milling in corundum jars and using corundum balls (series CSM). Since in series SSM a beneficial influence of sulfate ions on the formation of anatase was observed, all samples milled in corundum were annealed in the presence of a sulfate salt matrix. In samples milled in corundum and annealed in the temperature range of 300–700 °C the anatase crystalline phase is evidenced by XRD. Evidently also in this case the rutilization reaction is strongly inhibited by the presence of sulfate anions in the salt matrix during the annealing reaction. The size of anatase nanocrystallites increases with rising temperature (Table 1).

In all of the above cases if the samples were annealed at temperatures ≥300 °C, crystalline anatase or rutile phases were identified by XRD. The growth of the crystals in the heating process leads consecutively to consumption of the amorphous TiO_2 precursor. Therefore it can be expected that especially in samples annealed at lower temperatures, in which small titania nanocrystals were detected by XRD, a significant amount of amorphous titania is present. A similar process was observed in titania prepared by the sol–gel technique or under hydrothermal conditions [36,37].

3.2. TEM study of samples

The preliminary result of our studies of photoinduced activity showed that the samples milled in corundum show a higher initial rate of hydroxyl radical adduct formation ($^{\bullet}$DMPO-OH) than those

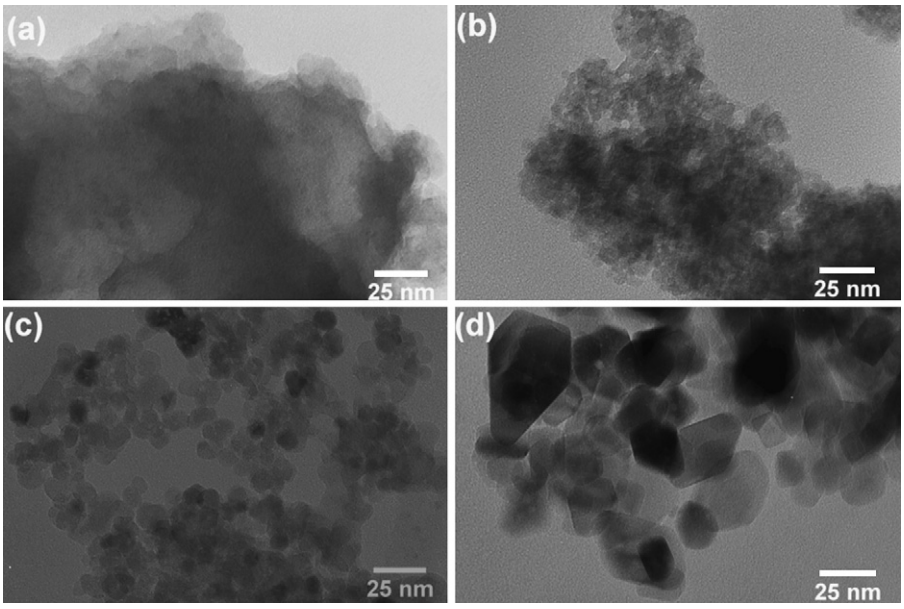

Fig. 1. TEM images of nanopowders milled in corundum (series CSM). (a) Seeded as-milled powder; anatase nanocrystallites evolved upon annealing at (b) 400 °C; (c) 500 °C; (d) 700 °C.

milled in steel [26]. Since the aim of our paper was to study the influence of structure on photoinduced activity, only the samples milled in corundum (series CSM) were studied in detail with TEM microscopy. The as-milled non-annealed amorphous product consists of irregularly shaped particles with sizes ranging from 50 to 400 nm (Fig. 1a). The TEM images are consistent with the formation of fine nanocrystallite aggregates upon calcination at 300 and 400 °C, respectively. The beginning of disaggregation of the original particles had been found in the agglomerate surface layers upon annealing at 400 °C. The majority of nanocrystallites assembled in the aggregates have a size of approximately 3 nm upon annealing at 300 °C. The heat treatment at 400 °C did not affect the crystallite size substantially compared with those annealed at 300 °C; the mean dimension of nanocrystallites was about 4–12 nm, with maximum at 6 nm (Fig. 1b).

Calcination at 500 °C leads to samples which consist predominantly of separated, rounded, spherical-like anatase nanocrystallites with mean diameters ranging from 7 to 25 nm; however most nanocrystals show a size of 13 nm (Fig. 1c).

The size and morphology of the nanocrystals obtained by the total breakdown of the as-milled amorphous TiO_2 powder after heating at 600 and 700 °C can be seen in Fig. 1d. It was established that the average crystallite size was in the range of 25–30 nm upon annealing at 600 and 700 °C, respectively. The preliminary isometric nanocrystallites, evolved by annealing at 500 °C, grew markedly upon heat treatment at 600 °C; however, their faceting occurred predominantly during calcination at a temperature of 700 °C (Fig. 1d). For the range of annealing temperatures 300–700 °C the size of the nanocrystallites calculated from the width of XRD diffraction is in good agreement with the crystallite size determined from TEM observation.

3.3. EPR spectra of powder titania samples

The utilization of steel jars for the mechanochemically induced reactions caused contamination of synthesized titania samples with transition metal ions originating from the oxidation of stainless steel elements (e.g., iron, chromium, nickel) [15,36–39]. Fig. 2 shows the EPR spectra of TiO_2 powders prepared in series S measured at 100 and 298 K. EPR spectra of samples S200–S600 annealed in the temperature range 200–600 °C are characterized by sharp spectral component at magnetic field 150 mT ($g_{eff} \sim 4.3$) and overlapping broad signals at 300 mT ($g_{eff} \sim 2.2$) and 335 mT ($g_{eff} \sim 2.0$). The EPR signal at $g_{eff} \sim 4.3$, which is significantly temperature dependent (see Fig. 2a and b), was previously attributed to the surface-Fe(III) ions dispersed on the surface of the titania nanoparticles, representing isolated Fe(III) ions in a distorted tetrahedral coordination [38–42]. The EPR signal at $g_{eff} \sim 2.0$ was attributed in the literature to bulk-Fe(III) centers [38–42], Fe(III) ions in octahedral symmetry of anatase structure [43], or chromium ions in various oxidation states [44–47]. The broad spectral component at $g_{eff} \sim 2.2$ was assigned to iron oxide aggregates, considered to be a close association of Fe(III) ions [48]. Consequently its linewidth monitored in EPR spectra can be affected by magnetic exchange coupling of interacting Fe(III) ions [42]. The EPR signals observed in the low temperature spectra of samples S700 and S800 (Fig. 2a) are compatible with paramagnetic signals assigned to Fe(III) or Cr(III) ions occupying cation sites vacated by Ti(IV) ions in a rutile matrix [39,40,44,49]. In this case the higher annealing temperature led to the incorporation of transition metal ions into the crystal structure of titania and the Fe(III) and Cr(III) ions are well separated in the lattice. Narrow signals from the EPR fine structure can be observed.

The determination of surface-Fe(III) concentration summarized in Fig. 3 shows that mechanochemical synthesis leads to products in which some contamination from the milling media remain on the surface of the obtained crystallites as the presence of surface-Fe(III) was evidenced in all TiO_2 samples milled in steel (35–7 ppm in series S, 45–20 ppm in series SSM). On the other hand, the transition metal ion surface concentration was negligible when the mechanochemical synthesis was performed in corundum jars (<3 ppm of surface-Fe(III) in series CSM).

3.4. UV/vis spectra of synthesized TiO_2 samples

The spectrophotometrically monitored extinction in heterogeneous titanium dioxide aqueous suspensions represents a combination of absorption and scattering caused by particles [32,33,50–55]:

$$E^{\lambda} = \beta^{\lambda} cl = (\varepsilon^{\lambda}_{abs} + \varepsilon^{\lambda}_{scat})cl \quad (2)$$

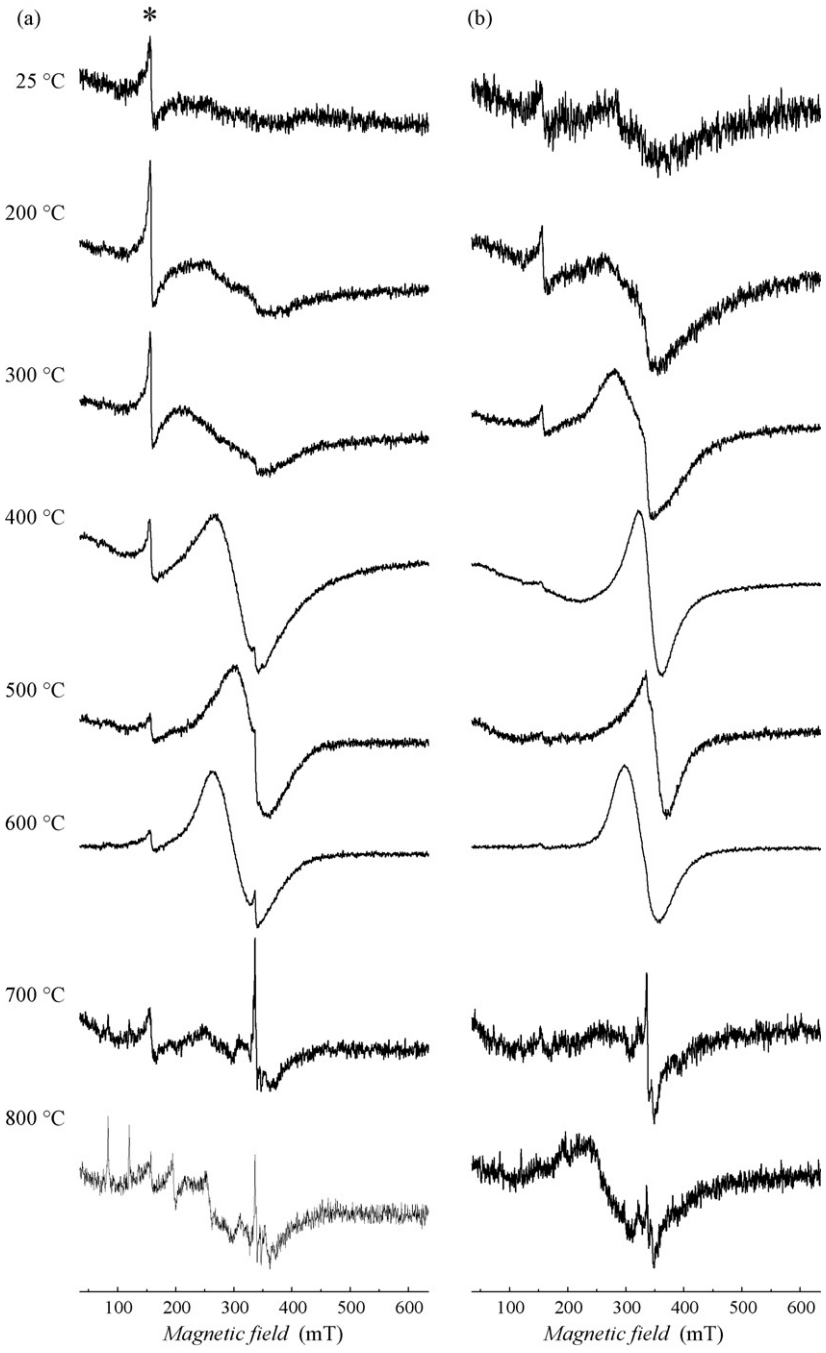

Fig. 2. EPR spectra of synthesized TiO_2 powders (S25–S800) annealed at specified temperatures measured at: (a) 100 K; (b) 298 K. (EPR signal marked with '*' having $g_{eff} = 4.3$ was attributed to surface-Fe(III) ions).

where E^{λ} is the extinction at a given wavelength λ; β^{λ} is the extinction coefficient ($cm^2\,g^{-1}$); $\varepsilon^{\lambda}_{abs}$, $\varepsilon^{\lambda}_{scat}$ are absorption and scattering coefficients, respectively ($cm^2\,g^{-1}$); c is the titanium dioxide concentration ($g\,cm^{-3}$); l is the optical path length (cm).

The band-gap energies of TiO_2 polymorphs (anatase, $E_{bg} = 3.2$ eV; rutile, $E_{bg} = 3.02$ eV) predetermine TiO_2 absorption of UV radiation only; consequently, the extinction observed in the visible region originates from scattering on titanium dioxide particles [32,33]. In samples S600–S800 the higher annealing temperatures (600–800 °C) lead to rising rutile content, which is manifested by the lower values of E_{bg} compared to S-series samples annealed in the temperature range 300–500 °C (Table 1).

Fig. 4 shows the experimental extinction spectra obtained for the TiO_2 samples synthesized in series CSM, in comparison to P25 Aeroxide®. The experimental data demonstrated that the temperature of post-milled annealing influences the optical properties of mechanochemically synthesized titania, since samples annealed below 700 °C (CSM300–CSM600) revealed a lower extinction than sample CSM700 (Fig. 4).

However, the highest extinction in the wavelength interval 240–400 nm was found for suspensions of P25 Aeroxide®, and data observed here for wavelengths $\lambda > 410$ nm are in a good agreement with Rayleigh scattering on P25 particles (extinction $= k \times \lambda^{-4}$) as has been described by Vione et al. [32]. Previously, the high extinction of Aeroxide® P25 in the wavelength interval 300–400 nm has been attributed to a substantial scattering phenomenon, and the values of the P25 scattering coefficients published for this spectral region were larger than 40 000 $cm^2\,g^{-1}$ [50].

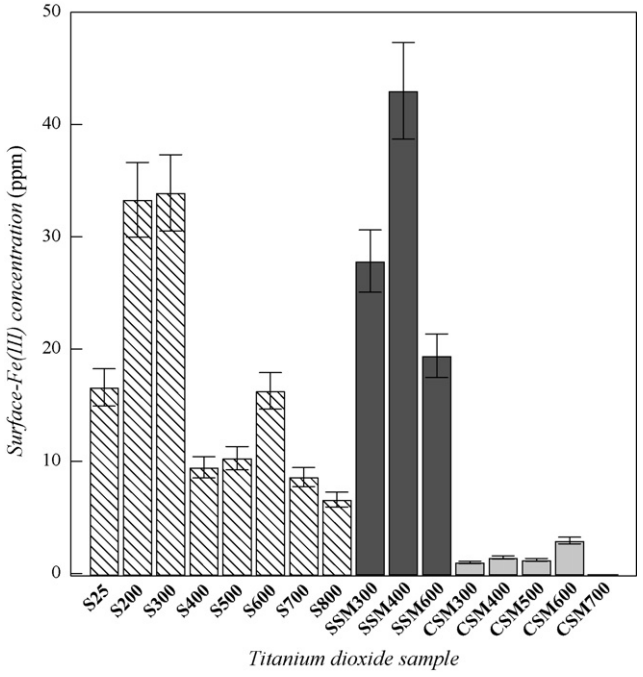

Fig. 3. Concentration of surface-Fe(III) ions in mechanochemically synthesized TiO_2 samples evaluated from EPR spectra recorded at 100 K (series CSM was milled using corundum, series SSM and S using stainless steel balls and jars, respectively).

In our investigation, the extinction spectra of titanium dioxide suspensions measured at various loadings were used to compute $\varepsilon^{\lambda}_{abs}$ and $\varepsilon^{\lambda}_{scat}$ in accordance with the Kubelka-Munk model of diffuse reflectance and transmission [32,33]. The values of absorption and scattering coefficients were evaluated at individual wavelengths (λ = 240–600 nm; with $\Delta\lambda$ = 5 nm). Fig. 5 shows the experimental extinction data found at λ = 365 nm for the CSM series and P25, along with their fitting to the theoretical Kubelka-Munk model [32,33]. The obtained values of $\varepsilon^{\lambda}_{abs}$ and $\varepsilon^{\lambda}_{scat}$ were used to construct the absorption and scattering spectra, i.e., $\varepsilon^{\lambda}_{abs} = f(\lambda)$, $\varepsilon^{\lambda}_{scat} = f(\lambda)$, of all TiO_2 samples investigated in the wavelength interval

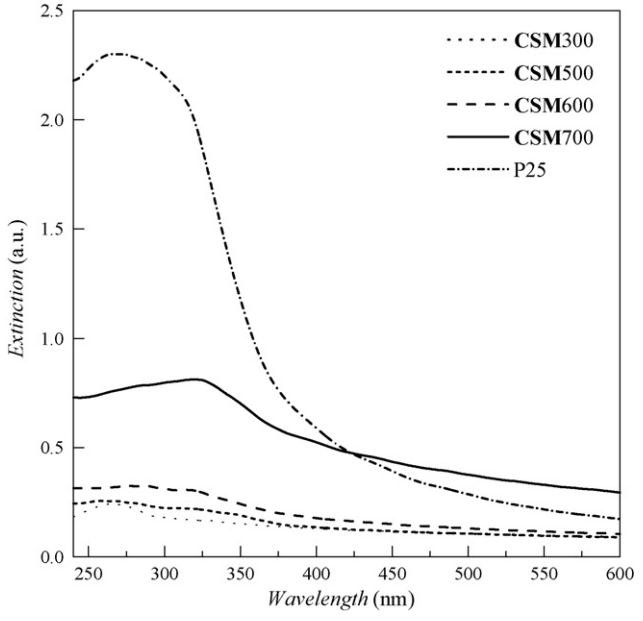

Fig. 4. UV/vis spectra, measured in aqueous suspensions, of titania samples CSM300, CSM500, CSM600, CSM700 and Aeroxide® P25 (TiO_2 concentration 5×10^{-5} g cm^{-3}).

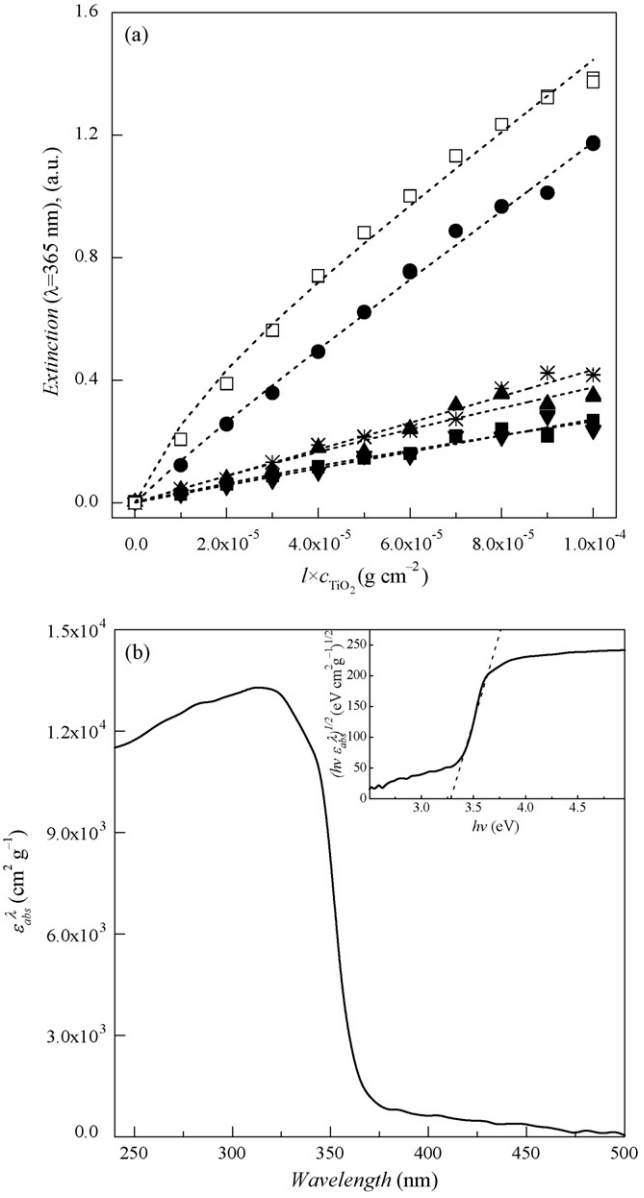

Fig. 5. The dependence of extinction at λ = 365 nm upon the product of cell length and TiO_2 concentration ($l \times c_{TiO_2}$) obtained for titanium dioxide samples: (□) Aeroxide® P25; (■) CSM300; (▼) CSM400; (▲) CSM500; (∗) CSM600; (●) CSM700. The symbols represent experimental data and the dotted lines were calculated by a least-squares minimization procedure using the Kubelka-Munk absorption and scattering model. (b) The calculated absorption spectrum of the CSM700 sample. The inset shows the dependence of $(\varepsilon^{\lambda}_{abs}\, h\nu)^{1/2}$ on the photon energy (in eV) used in the evaluation of the TiO_2 band-gap energy (E_{bg}).

240–600 nm. Fig. 5b shows the calculated absorption spectrum of the CSM700 sample, along with a plot representing the dependence of $(\varepsilon^{\lambda}_{abs}\, h\nu)^{1/2}$ on photon energy with respect to indirect transitions, suitable for the evaluation of the TiO_2 band-gap energy (inset in Fig. 5b). The absorption edge of synthesized TiO_2 samples was calculated using Eq. (3) [56–59]:

$$\varepsilon^{\lambda}_{abs} h\nu = A(h\nu - E_{bg})^{m} \quad (3)$$

where A is constant; m is 1/2 or 2 for direct or indirect transitions, respectively.

The linear segment in the dependence of $(\varepsilon^{\lambda}_{abs}\, h\nu)^{1/2}$ on photon energy ($h\nu$) evidences the existence of allowed indirect transitions [56–59]. The values of E_{bg} were evaluated from the point of inter-

section of the linear dependence with photon energy axis assuming $\varepsilon^{\lambda}_{abs} = 0$ (inset in Fig. 5b).

The spectral data found for mechanochemically synthesized titania confirmed a significant effect of post-milling annealing temperature on the absorption/scattering coefficients at $\lambda = 365$ nm (Table 1). Most likely, the absorption and scattering phenomena are determined by the actual size of titania clusters in the suspension which are affected by the particle size of the nanopowders and their ability to generate aggregates in aqueous media [60]. It should be noted here that the values obtained in our experiments for P25 Aeroxide®, i.e., the absorption coefficient value $\varepsilon^{365}_{abs} = 1100\,cm^2\,g^{-1}$ and $\varepsilon^{365}_{scat} = 37\,000\,cm^2\,g^{-1}$, are in good agreement with previously published results [32,50].

3.5. Photoinduced activity of mechanochemically synthesized TiO_2 powders

3.5.1. In situ EPR spin trapping experiments

The photoinduced formation of reactive oxygen-centered free radicals in the aerated TiO_2 aqueous suspensions was investigated using an EPR spin trapping technique, a suitable method for indirect detection of short-lived radicals [61]. Upon UVA irradiation of aerated TiO_2 suspensions in the presence of DMPO, typical four-line EPR spectra were monitored (Fig. 6a), which are characterized by the spin Hamiltonian parameters $a_N = 1.495$ mT, $a^{\beta}_H = 1.472$ mT; $g = 2.0057$, and are representative of the hydroxyl radical added to DMPO (•DMPO-OH). The formation of hydroxyl radical spin adducts was also evidenced using DIPPMPO, as the characteristic EPR spectrum of hydroxyl radical adduct (•DIPPMPO-OH; $a_N = 1.407$ mT, $a^{\beta}_H = 1.320$ mT, $a_P = 4.665$; $g = 2.0058$) was observed upon photoexcitation of TiO_2 in aqueous media (Fig. 6b).

The experimental sets of EPR spectra, monitored *in situ* upon continuous irradiation of aerated TiO_2 suspensions as well as TiO_2-free solution in the presence of DMPO or DIPPMPO, are shown in Fig. 7. The relative integral intensities of the •DMPO-OH adduct were calculated by double-integration of the individual experimental spectra, and the adduct concentrations upon UVA exposure were determined. The obtained dependencies of •DMPO-OH concentration upon irradiation time (t_{irr}) were fitted by a non-linear least-squares method to the formal kinetic models (first-order or consecutive first-order kinetics when a decrease of •DMPO-OH concentration upon irradiation was observed), and the initial rate of photoinduced •DMPO-OH formation was calculated (4):

$$R_{in}(\text{•DMPO-OH}) = \left(\frac{dc(\text{•DMPO-OH})}{dt_{irr}}\right)_{t_{irr}\to 0} \quad (4)$$

Under the given experimental conditions of monitoring the photoinduced radical processes by an *in situ* EPR technique, the TiO_2 suspensions were irradiated in an EPR flat cell with a very low optical path length of 0.045 cm. Consequently, the calculation of photonic yield considering the UVA photons flux absorbed by titania [62], were approximated in our computations with photonic efficiency taking into account the incident UVA photon flux in accordance with Ref. [63].

The values of R_{in}(•DMPO-OH) served as a basis for the computation of the UVA photonic efficiency of •DMPO-OH formation for all synthesized TiO_2 samples (5):

$$\xi_{UVA} = \frac{R_{in}}{\phi^{UVA}_{inc}} \quad (5)$$

where ϕ^{UVA}_{inc} represents the incident UVA photon flux (1.8×10^{-8} Einstein s^{-1}).

The paramagnetic signal of •DMPO-OH adduct may be produced directly by the addition of photoproduced hydroxyl radicals; however, we cannot exclude alternative mechanisms without direct

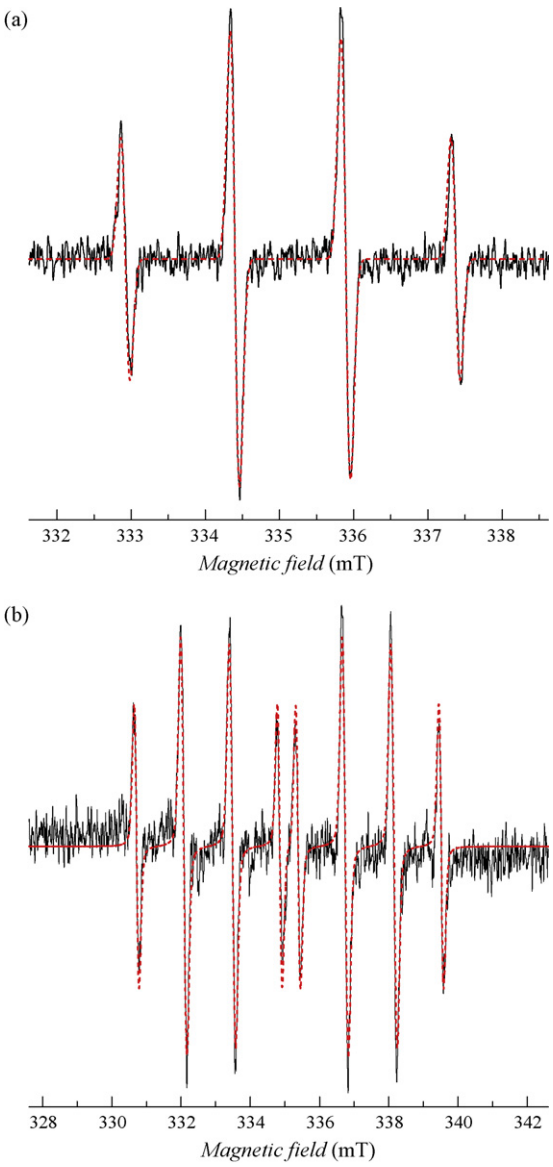

Fig. 6. Experimental (black line) and simulated (red line) EPR spectra obtained in the aerated irradiated TiO_2 suspensions in the presence of spin trapping agents: (a) DMPO; (b) DIPPMPO. (TiO_2 concentration 5×10^{-4} g cm^{-3}, initial spin trap concentrations $c_{0,DMPO} = 0.025$ M; $c_{0,DIPPMPO} = 0.01$ M.) Simulation spectra were calculated using spin Hamiltonian parameters corresponding to addition of hydroxyl radical, i.e., •DMPO-OH ($a_N = 1.495$ mT, $a^{\beta}_H = 1.472$ mT; $g = 2.0057$) and •DIPPMPO-OH ($a_N = 1.407$ mT, $a^{\beta}_H = 1.320$ mT, $a_P = 4.665$; $g = 2.0058$). (For interpretation of the references to colour in this figure legend, the reader is referred to the web version of the article.)

hydroxyl radical formation [24,63]. Previously, Nosaka et al. investigated hydroxyl radical formation in TiO_2 suspensions using EPR spectroscopy (DMPO spin trapping technique, spin probe assay with termination of nitroxide radicals), or fluorescence intensity measurements (specific hydroxyterephthalic acid formation *via* •OH radicals), assuming an incident light flux in the calculation of "apparent quantum efficiency" [63]. The results pointed to the formation of •DMPO-OH adducts *via* different mechanisms (i.e., direct hydroxyl radical addition or trapped holes oxidation) as the fluorescence quantum efficiency, corresponding to the direct reaction of hydroxyl radicals with terephthalic acid, was significantly lower than those found by spin trapping or spin probe techniques [63].

Fig. 8a summarizes the values of UVA photonic efficiency of •DMPO-OH formation for all the investigated TiO_2 samples. The

highest ability to produce •DMPO-OH spin adducts upon UVA irradiation was found for sample CSM700, exceeding the value found for Aeroxide® P25.

3.5.2. Photoinduced reduction of the radical cation ABTS•+

An alternative assay to determine the photoinduced activity of synthesized titania samples consists of photoinduced termination of the paramagnetic radical cation ABTS•+ (inset in Fig. 8b), monitoring *in situ* the decrease of EPR signal intensity of ABTS•+ upon continuous irradiation of titanium dioxide suspensions [24]. The monitored decrease in ABTS•+ concentration was described by formal first-order kinetics, allowing extraction of the initial rate of ABTS•+ termination, R_{in}(ABTS•+). Recently, our UV/vis experiments confirmed that the process of ABTS•+ radical cation termination in Aeroxide® P25 suspensions is coupled with its reduction to the parent diamagnetic compound ABTS by electrons photogenerated upon TiO_2 excitation [24]. The photoinduced electron transfer was also confirmed here as the UV/vis spectra showed a decrease of the ABTS•+ selective absorption bands at 735 and 415 nm, and simultaneous growth of the ABTS absorption at 340 nm, with an isosbestic point at 368 nm, in good correlation with the reduction of the radical cation ABTS•+ to ABTS as shown Fig. 9a. On the other hand, irradiation of TiO_2-free homogeneous solution of ABTS•+ caused only a 5% decrease of the radical cation concentration after a 600-s exposure (Fig. 9b). The values of UVA photonic efficiency of ABTS•+ reduction calculated using Eq. (5) (Fig. 8b), are approximately 10 times higher than the photonic efficiencies found using •DMPO-OH (Fig. 8a), and prove that radical cation ABTS•+ behaves as an effective electron-scavenger under the given experimental conditions. We assume that in the photoinduced reduction of ABTS•+, the surface properties of synthesized titania powders play an important role, influencing the adsorption of radical cations on the surface. A linear correlation was observed between UVA photonic efficiencies found *via* paramagnetic species •DMPO-OH and ABTS•+ with correlation coefficient $r = 0.927$ at a 95% confidence level shown in Fig. 8c.

Colón et al. showed that the sulfation of TiO_2 under mild conditions remarkably increases its photocatalytic properties after annealing at 700 °C [35]. In a later paper [64] they ascribed this effect to the formation of oxygen vacancies in the process of annealing and the formation of a highly defect surface. This would explain the enhancement of catalytic activity by improvement of charge separation on surface. In our investigations the sulfate precursor was used for the synthesis of nanocrystalline TiO_2. The sample series SSM and CSM were even heated in presence of a sulfate matrix. It is possible that, among other factors, the effect of TiO_2 surface interaction with sulfates could be responsible for the effective radical formation on the nanopowders under investigation. However, the detailed description of this effect would require further studies.

The mechanochemical synthesis always leads to some contamination of the product surface by milling elements. Different results on the effect of iron ion doping on the photoinduced activity of titanium dioxide have been reported previously [65,66]. Obviously the effect of iron doping depends on the method of synthesis, which crucially influences the structure of nanoparticles. According to [67,68] the effect of iron doping in TiO_2 crucially depends on its concentration. At low concentration iron alleviates the formation of hole and electron traps, reduces the h^+/e^- recombination and consequently increases the photoactivity. On the other hand at higher doping levels iron can act as a recombination centre for electron/hole pairs resulting in decreased photocatalytic activity. The values of photonic efficiencies found in our study evidence that the surface-Fe(III) ions in the concentration range below 50 ppm exhibit only a partial effect on the photoactivity of mechanochemically synthesized titania powders considering the complex phenomena of heterogeneous photoprocesses. The phase composition of prepared titania was remarkably influenced by presence of iron but the

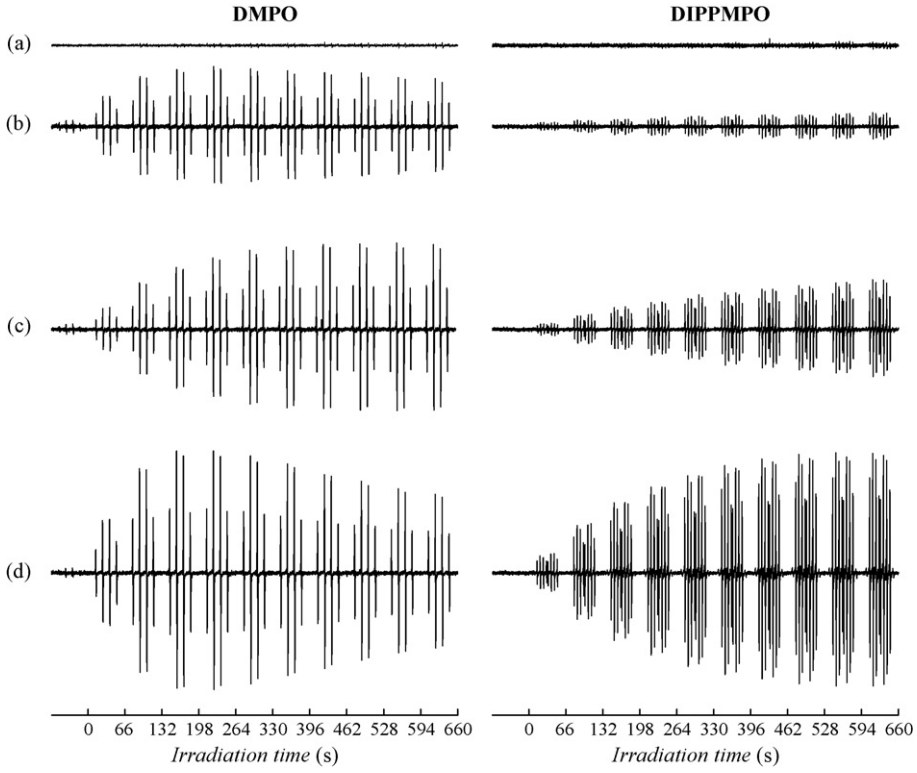

Fig. 7. The sets of individual EPR spectra monitored upon continuous irradiation of aerated TiO_2 suspensions in the presence of spin trapping agents DMPO and DIPPMPO (TiO_2 concentration 5×10^{-4} g cm^{-3}, $c_{0,DMPO} = 0.025$ M; $c_{0,DIPPMPO} = 0.01$ M). (a) TiO_2-free system; (b) Aeroxide® P25; (c) CSM600; (d) CSM700.

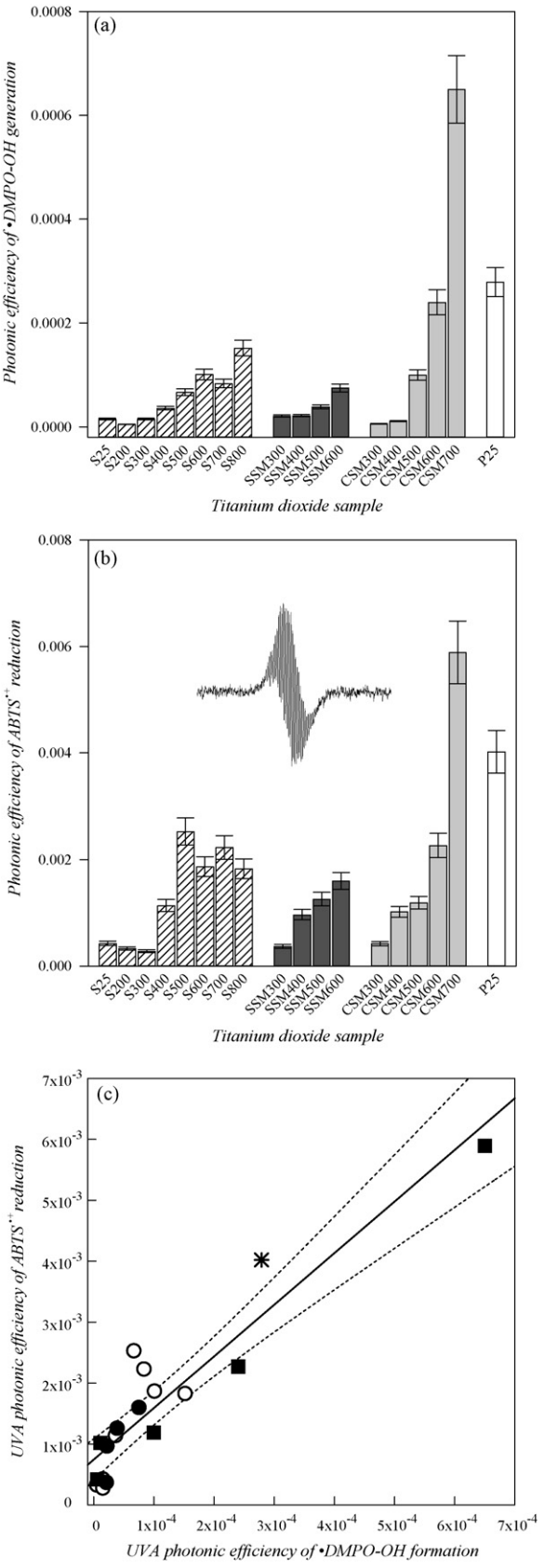

Fig. 8. The values of UVA photonic efficiency of photoinduced processes using mechanochemically synthesized TiO_2 samples and Aeroxide® P25: (a) •DMPO-OH formation; (b) $ABTS^{\bullet+}$ reduction (inset shows the EPR spectrum of $ABTS^{\bullet+}$ over 10 mT magnetic field sweep); (c) the linear relationship at a 95% confidence level (confidence bands marked with dotted lines) between UVA photonic efficiency of •DMPO-OH formation and UVA photonic efficiency of $ABTS^{\bullet+}$ reduction (○ S; ● SSM; ■ CSM; ∗ P25).

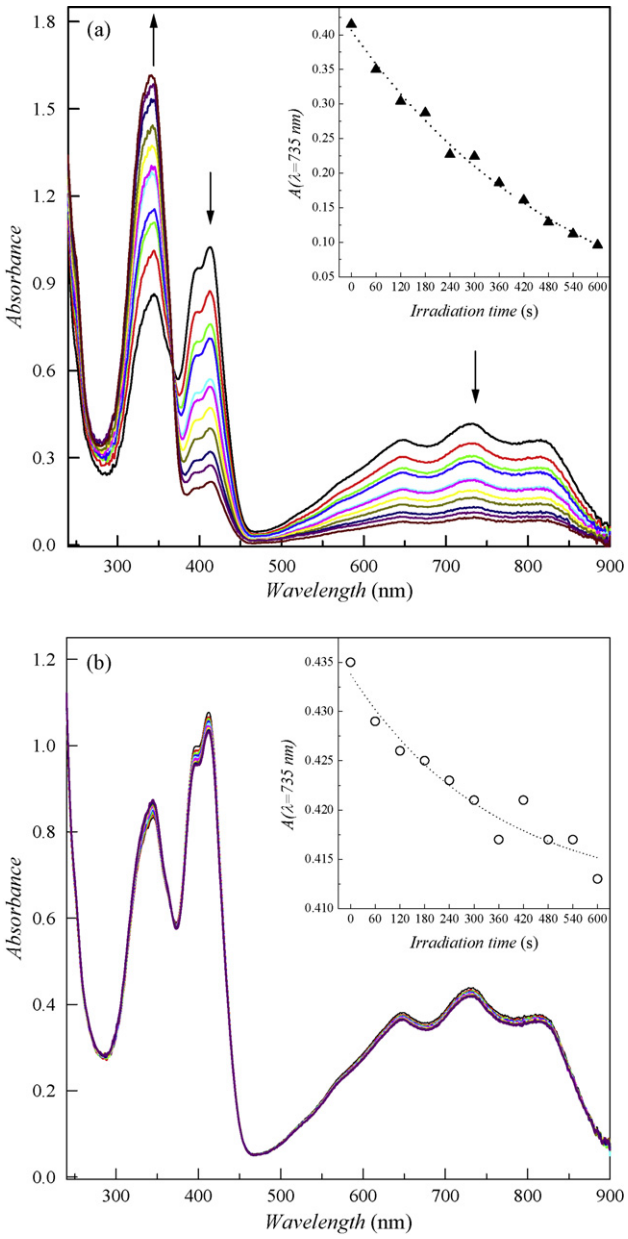

Fig. 9. Changes in the UV/vis spectra measured upon irradiation of radical cation $ABTS^{\bullet+}$ ($c_{0,ABTS^{\bullet+}} = 30\,\mu M$) in: (a) titanium dioxide CSM500 aqueous suspensions (TiO_2 concentration $1 \times 10^{-4}\,g\,cm^{-3}$); (b) TiO_2-free solution. The insets represent decline of absorbance at $\lambda = 735$ nm characteristic for $ABTS^{\bullet+}$ (the UV/vis spectra were recorded using a large integrating sphere assembly with transmittance measurement accessory using as reference analogous TiO_2 suspension or distilled water, respectively).

character of annealing temperature dependence of photoactivity was similar in all series of samples. Among the iron-containing samples the series S, with higher content of rutile, exhibits improved photoactivity compared with the series SSM which has a lower rutile content. This could be ascribed to the enhancement of photocatalytic activity by "antenna effect" [69]—the interphase charge transfer in two phase anatase/rutile system. It has been reported that alumina admixture up to 4 wt% increases the photocatalytic activity of titania [70]. In the samples milled in corundum the contamination of products with alumina from milling tools was below the detection limit of EDX (<0.1 wt%). The above results allow us to conclude that, in mechanochemically prepared titania nanopowders with low impurity levels, the prevailing influence on

the photocatalytic activity is the TiO_2 crystal structure and size and shape of crystallites.

4. Conclusions

Solvent-free mechanochemical synthesis in a high-energy ball mill with subsequent annealing of the as-milled samples represents a promising technique for the preparation of titania nanopowders with various structures and photoactivities. The production of anatase TiO_2 materials with high photoactivity requires the elimination of transition metal ion contamination during the milling procedure. Under given experimental conditions the iron ions probably act as radical recombination centers and decrease the efficiency of monitored photoinduced radical processes. In addition, the presence of iron and chromium ions also increases the content of rutile allotrope in the mechanochemically synthesized titania powders.

The samples with high photocatalytic activity were prepared by milling the $TiOSO_4{\cdot}xH_2O$ and Na_2CO_3 precursors in corundum and subsequent annealing of the amorphous product in the presence of a sulfate salt matrix at temperatures in the range of 600–700 °C. At 700 °C well faceted anatase nanocrystals with a size between 25 and 30 nm are formed. Generally it is accepted that the faceting of the nanocrystals is one of the crucial factors improving the photocatalytic activity of anatase [37,71]. The rise of annealing temperature from 600 to 700 °C caused only negligible enlargement of crystals, however, a remarkable improvement of faceting occurred. It allows us to assume that the well-developed faceting of our samples prepared on corundum and annealed at 700 °C remarkably improves the photoactivity as monitored by EPR. The results obtained in the study of photoinduced formation of hydroxyl radical spin adducts using an EPR spin trapping technique show a linear correlation with those found by photoinduced reduction of the paramagnetic radical cation $ABTS^{\bullet+}$ in aerated TiO_2 aqueous suspensions.

Acknowledgements

The authors wish to thank to Science and Technology Assistance Agency Slovakia (project APVV-VVCE-003307) and the Scientific Grant Agency of the Slovak Republic (Project VEGA/1/0018/09 and VEGA 1/0337/08) for financial support. We thank Marián Valko, Milan Mazúr and Harry Morris for helpful discussion and the referees for valuable comments.

References

[1] U.I. Gaya, A.H. Abdullah, Heterogeneous photocatalytic degradation of organic contaminants over titanium dioxide: a review of fundamentals, progress and problems, J. Photochem. Photobiol. C: Photochem. Rev. 9 (2008) 1–12.
[2] L. Zhang, P. Li, Z. Gong, X. Li, Photocatalytic degradation of polycyclic aromatic hydrocarbons on soil surfaces using TiO_2 under UV light, J. Hazard. Mater. 158 (2008) 478–484.
[3] C.M. Schmidt, A.M. Buchbinder, E. Weitz, F.M. Geiger, Photochemistry of the indoor air pollutant acetone on Degussa P25 TiO_2 studied by chemical ionization mass spectrometry, J. Phys. Chem. A 111 (2007) 13023–13031.
[4] H. Wang, J. Yan, W. Chang, Z. Zhang, Practical synthesis of aromatic amines by photocatalytic reduction of aromatic nitro compounds on nanoparticles N-doped TiO_2, Catal. Commun. 10 (2009) 989–994.
[5] A.R. Suresh Babu, R. Raghunathan, TiO_2-mediated, one-pot, four-component 1,3-dipolar cycloaddition reaction: a facile synthesis of dispiro-pyrrolidine ring systems, Synth. Commun. 39 (2009) 347–354.
[6] V. Augugliaro, H. Kisch, V. Loddo, M.J. Lopez-Muñoz, C. Marquez-Alvarez, G. Palmisano, L. Palmisano, F. Parrino, S. Yurdakal, Photocatalytic oxidation of aromatic alcohols to aldehydes in aqueous suspension of home-prepared titanium dioxide. 1. Selectivity enhancement by aliphatic alcohols, Appl. Catal. A: Gen. 349 (2008) 182–188.
[7] Z. Liu, X. Zhang, T. Murakami, A. Fujishima, Sol–gel SiO_2/TiO_2 bilayer films with self-cleaning and antireflection properties, Solar Energy Mater. Solar Cells 92 (2008) 1434–1438.
[8] A. Borras, A. Barranco, A.R. Gonzalez-Elipe, Reversible superhydrophobic to superhydrophilic conversion of $Ag@TiO_2$ composite nanofiber surfaces, Langmuir 24 (2008) 8021–8026.
[9] M. Shirolkar, M.K. Abyaneh, A. Singh, A. Tomer, R. Choudhary, V. Sathe, D. Phase, S. Kulkarni, Rapidly switched wettability of titania films deposited by dc magnetron sputtering, J. Phys. D: Appl. Phys. 41 (2008), art. no. 155308.
[10] J. Soria, J. Sanz, I. Sobrados, J.M. Coronado, F. Fresno, M.D. Hernandez-Alonso, Magnetic resonance study of the defects influence on the surface characteristics of nanosize anatase, Catal. Today 129 (2007) 240–246.
[11] M.D. Hernandez-Alonso, I. Tejedor-Tejedor, J.M. Coronado, J. Soria, M.A. Anderson, Sol–gel preparation of TiO_2–ZrO_2 thin films supported on glass rings: influence of phase composition on photocatalytic activity, Thin Solid Films 502 (2006) 125–131.
[12] K.L. Yeung, S.T. Yau, A.J. Maira, J.M. Coronado, J. Soria, P.L. Yue, The influence of surface properties on the photocatalytic activity of nanostructured TiO_2, J. Catal. 219 (2003) 107–116.
[13] J.M. Coronado, J. Soria, ESR study of the initial stages of the photocatalytic oxidation of toluene over TiO_2 powders, Catal. Today 123 (2007) 37–41.
[14] J.M. Coronado, A. Javier Maira, A. Martinez-Arias, J.C. Conesa, J. Soria, EPR study of the radicals formed upon UV irradiation of ceria-based photocatalysts, J. Photochem. Photobiol. A: Chem. 150 (2002) 213–221.
[15] D. Dvoranová, V. Brezová, M. Mazúr, M.A. Malati, Investigations of metal-doped titanium dioxide photocatalysts, Appl. Catal. B: Environ. 37 (2002) 91–105.
[16] N.M. Dimitrijevic, Z.V. Saponjic, B.M. Rabatic, O.G. Poluektov, T. Rajh, Effect of size and shape of nanocrystalline TiO_2 on photogenerated charges, an EPR study, J. Phys. Chem. C 111 (2007) 14597–14601.
[17] R. Scotti, I.R. Bellobono, C. Canevali, C. Cannas, M. Catti, M. D'Arienzo, A. Musinu, S. Polizzi, M. Sommariva, A. Testino, F. Morazzoni, Sol–gel pure and mixed-phase titanium dioxide for photocatalytic purposes: relations between phase composition, catalytic activity, and charge-trapped sites, Chem. Mater. 20 (2008) 4051–4061.
[18] E. Carter, A.F. Carley, D.M. Murphy, Evidence for O_2^- radical stabilization at surface oxygen vacancies on polycrystalline TiO_2, J. Phys. Chem. C 111 (2007) 10630–10638.
[19] C.D. Jaeger, A.J. Bard, Spin trapping and electron spin resonance detection of radical intermediates in the photodecomposition of water at TiO_2 particulate systems, J. Phys. Chem. 83 (1979) 3146–3152.
[20] G. Riegel, J.R. Bolton, Photocatalytic efficiency variability in TiO_2 particles, J. Phys. Chem. 99 (1995) 4215–4224.
[21] R. Konaka, E. Kasahara, W.C. Dunlap, Y. Yamamoto, K.C. Chien, M. Inoue, Ultraviolet irradiation of titanium dioxide in aqueous dispersion generates singlet oxygen, Redox Rep. 6 (2001) 319–325.
[22] R. Konaka, E. Kasahara, W.C. Dunlap, Y. Yamamoto, K.C. Chien, M. Inoue, Irradiation of titanium dioxide generates both singlet oxygen and superoxide anion, Free Radic. Biol. Med. 27 (1999) 294–300.
[23] V. Brezová, A. Staško, S. Biskupič, A. Blažková, B. Havlínová, Kinetics of hydroxyl radical spin trapping in photoactivated homogeneous (H_2O_2) and heterogeneous (TiO_2, O_2) aqueous systems, J. Phys. Chem. 98 (1994) 8977–8984.
[24] V. Brezová, D. Dvoranová, A. Staško, Characterization of titanium dioxide photoactivity following the formation of radicals by EPR spectroscopy, Res. Chem. Intermed. 33 (2007) 251–268.
[25] A. Dodd, A. McKinley, T. Tsuzuki, M. Saunders, Optical and photocatalytic properties of nanocrystalline TiO_2 synthesised by solid-state chemical reaction, J. Phys. Chem. Solids 68 (2007) 2341–2348.
[26] P. Billik, G. Plesch, V. Brezová, Ľ. Kuchta, M. Valko, M. Mazúr, Anatase TiO_2 nanocrystals prepared by mechanochemical synthesis and their photochemical activity studied by EPR spectroscopy, J. Phys. Chem. Solids 68 (2007) 1112–1116.
[27] P. Billik, G. Plesch, Mechanochemical synthesis of anatase and rutile nanopowders from $TiOSO_4$, Mater. Lett. 61 (2007) 1183–1186.
[28] P. Billik, G. Plesch, Mechanochemical synthesis of nanocrystalline TiO_2 from liquid $TiCl_4$, Scripta Mater. 56 (2007) 979–982.
[29] M. Salari, S.M. Mousavi khoie, P. Marashi, M. Rezaee, Synthesis of TiO_2 nanoparticles via a novel mechanochemical method, J. Alloys Comp. 469 (2009) 386–390.
[30] X. Ni, J. Ma, J. Li, D. Jiao, J. Huang, X. Zhang, Microwave characteristics of Co/TiO_2 nanocomposites prepared by mechanochemical synthesis, J. Alloys Comp. 468 (2009) 386–391.
[31] K. Okada, N. Yamamoto, Y. Kameshima, A. Yasumori, K.J.D. MacKenzie, Effect of silica additive on the anatase-to-rutile transformation, J. Am. Ceram. Soc. 84 (2001) 1591–1596.
[32] D. Vione, C. Minero, V. Maurino, M.E. Carlotti, T. Picatonotto, E. Pelizzetti, Degradation of phenol and benzoic acid in the presence of a TiO_2-based heterogeneous photocatalyst, Appl. Catal. B: Environ. 58 (2005) 79–85.
[33] L.E. McNeil, R.H. French, Multiple scattering from rutile TiO_2 particles, Acta Mater. 48 (2000) 4571–4576.
[34] M. Kanna, S. Wongnawa, Mixed amorphous and nanocrystalline TiO_2 powders prepared by sol–gel method: characterization and photocatalytic study, Mater. Chem. Phys. 110 (2008) 166–175.
[35] G. Colón, M.C. Hidalgo, J.A. Navío, Photocatalytic behaviour of sulphated TiO_2 for phenol degradation, Appl. Catal. B 45 (2003) 39–50.
[36] Hari-Bala, Y. Guo, X. Zhao, J. Zhao, W. Fu, X. Ding, Y. Jiang, K. Yu, X. Lv, Z. Wang, Controlling the particle size of nanocrystalline titania via a thermal dissociation of substrates with ammonium chloride, Mater. Lett. 60 (2006) 494–498.
[37] C.H. Cho, M.H. Han, D.H. Kim, D.K. Kim, Morphology evolution of anatase TiO_2 nanocrystals under hydrothermal condition (pH = 9.5) and their ultra-high photo-catalytic activity, Mater. Chem. Phys. 92 (2005) 104–111.
[38] M. Zhou, J. Yu, B. Cheng, H. Yu, Preparation and photocatalytic activity of Fe-doped mesoporous titanium dioxide nanocrystalline photocatalysts, Mater. Chem. Phys. 93 (2005) 159–163.

[39] A. Amorelli, J.C. Evans, C.C. Rowlands, An electron spin resonance study of rutile and anatase titanium dioxide polycrystalline powders treated with transition-metal ions, J. Chem. Soc., Faraday Trans. 183 (1987) 3541–3548.
[40] A. Amorelli, J.C. Evans, C.C. Rowlands, Electron paramagnetic resonance study of transition-metal-ion impregnated brookite titanium dioxide powders, J. Chem. Soc., Faraday Trans. 185 (1987) 4031–4038.
[41] X. Li, P.-L. Yue, C. Kutal, Synthesis and photocatalytic oxidation properties of iron doped titanium dioxide nanosemiconductor particles, New J. Chem. 27 (2003) 1264–1269, 27.
[42] C. Adán, A. Bahamonde, M. Fernández-García, A. Martínez-Arias, Structure and activity of nanosized iron-doped anatase TiO_2 catalysts for phenol photocatalytic degradation, Appl. Catal. B: Environ. 72 (2007) 11–17.
[43] J. Zhu, F. Chen, J. Zhang, H. Chen, M. Anpo, Fe^{3+}–TiO_2 photocatalysts prepared by combining sol–gel method with hydrothermal treatment and their characterization, J. Photochem. Photobiol. A: Chem. 180 (2006) 196–204.
[44] K. Köhler, W. Mörke, T. Bieruta, Magnetic resonance (FMR, EPR) of chromium dioxide supported on titania, Colloids Surf. A: Physicochem. Eng. Aspects 144 (1998) 81–87.
[45] J.J. Testa, M.A. Grela, M.I. Litter, Experimental evidence in favor of an initial one-electron-transfer process in the heterogeneous photocatalytic reduction of chromium(VI) over TiO_2, Langmuir 17 (2002) 3515–3517.
[46] E. Abi Aad, A. Aboukaïs, Characterisation by EPR spectroscopy, Catal. Today 56 (2000) 371–378.
[47] Z. Sojka, M. Che, Catalytic chemistry of transition metal ions on oxide surfaces. A molecular approach using EPR techniques, C. R. Acad. Sci. Paris—Series IIc: Chem. 3 (2000) 163–174.
[48] A. Gervasini, C. Messi, P. Carniti, A. Ponti, N. Ravasio, F. Zaccheria, Insight into the properties of Fe oxide present in high concentrations on mesoporous silica, J. Catal. 262 (2009) 224–234.
[49] R.S. de Biasi, A.A.R. Fernandes, M.L.N. Grillo, Measurement of small concentrations of chromium and iron in the rutile (TiO_2) using electron spin resonance, J. Am. Ceram. Soc. 76 (1993) 223–225.
[50] M.I. Cabrera, O.M. Alfano, A.E. Cassano, Absorption and scattering coefficients of titanium dioxide particulate suspensions in water, J. Phys. Chem. 100 (1996) 20043–20050.
[51] D.W. Bahneman, M. Hilgendorff, R. Memming, Charge carrier dynamics at TiO_2 particles: reactivity of free and trapped holes, J. Phys. Chem. B 101 (1997) 4265–4275.
[52] B. Toepfer, A. Gora, G. Li Puma, Photocatalytic oxidation of multicomponent solutions of herbicides: reaction kinetics analysis with explicit photon absorption effects, Appl. Catal. B: Environ. 68 (2006) 171–180.
[53] C. Wang, J. Rabani, D.W. Bahneman, J.K. Dohrmann, Photonic efficiency and quantum yield of formaldehyde formation from methanol in the presence of various TiO_2 photocatalysts, J. Photochem. Photobiol. A: Chem. 148 (2002) 169–176.
[54] S. Yurdakal, V. Loddo, B.B. Ferrer, G. Palmisano, G. Palmisano, V. Augugliaro, J.G. Farreras, L. Palmisano, Optical properties of TiO_2 suspensions: influence of pH and powder concentration on mean particle size, Ind. Eng. Chem. Res. 46 (2007) 7620–7626.
[55] L. Sun, J.R. Bolton, Determination of the quantum yield for the photochemical generation of hydroxyl radicals in TiO_2 suspensions, J. Phys. Chem. 100 (1996) 4127–4134.
[56] M. Mikula, M. Čeppan, J. Kindernay, D. Búc, Photoelectrochemical properties of TiO_x layers prepared by DC pulsed unbalanced reactive magnetron sputtering, Czech. J. Phys. 49 (1999) 393–403.
[57] S. Tanemura, L. Miao, P. Jin, K. Kaneko, A. Terai, N. Nabatova-Gabain, Optical properties of polycrystalline and epitaxial anatase and rutile TiO_2 thin films by rf magnetron sputtering, Appl. Surf. Sci. 212–213 (2003) 654–660.
[58] K.M. Reddy, S.V. Manorama, A.R. Reddy, Bandgap studies on anatase titanium dioxide nanoparticles, Mater. Chem. Phys. 78 (2002) 239–245.
[59] M.-M. Abdel-Aziz, I.S. Yahia, L.A. Wahab, M. Fadel, M.A. Afifi, Determination and analysis of dispersive optical constant of TiO_2 and Ti_2O_3 thin films, Appl. Surf. Sci. 252 (2006) 8163–8170.
[60] C.A. Martín, M.A. Baltanás, A.E. Cassano, Photocatalytic reactors. I. Optical behavior of titanium oxide particulate suspensions, J. Photochem. Photobiol. A: Chem. 76 (1993) 199–208.
[61] A.S.W. Li, K.B. Cummings, H.P. Rothling, G.R. Buettner, C.F. Chignell, A spin-trapping database implemented on the IBM PC/AT, J. Magn. Reson. 79 (1988), 140, http://epr.niehs.nih.gov.
[62] V. Parmon, A.V. Emeline, N. Serpone, Glossary of terms in photocatalysis and radiocatalysis, Int. J. Photoenerg. 4 (2002) 91–131.
[63] Y. Nosaka, S. Komori, K. Yawata, T. Hirakawa, A.Y. Nosaka, Photocatalytic $^{\bullet}OH$ radical formation in TiO_2 aqueous suspension studied by several detection methods, Phys. Chem. Chem. Phys. 5 (2003) 4731–4735.
[64] G. Colón, M.C. Hidalgo, G. Munuera, I. Ferino, M.G. Cutrufello, J.A. Navío, Structural and surface approach to the enhanced photocatalytic activity of sulfated TiO_2 photocatalyst, Appl. Catal. B 63 (2006) 49–5950.
[65] M.I. Litter, J.A. Navío, Photocatalytic properties of iron-doped titania semiconductors, J. Photochem. Photobiol. A: Chem. 98 (1996) 171–181.
[66] J. Zhu, F. Chen, J. Zhan, H. Chen, M. Anpo, Fe^{3+}–TiO_2 photocatalysts prepared by combining sol–gel method with hydrothermal treatment and their characterization, J. Photochem. Photobiol. A: Chem. 180 (2006) 196–204.
[67] J. Zhu, W. Zheng, B. He, J. Zhang, M. Anpo, Characterization of Fe–TiO_2 photocatalysts synthesized by hydrothermal method and their photocatalytic reactivity for photodegradation of XRG dye diluted in water, J. Mol. Catal. A 216 (2004) 35–43.
[68] W.C. Hung, Y.C. Chen, H. Chu, T.K. Tseng, Synthesis and characterization of TiO_2 and Fe/TiO_2 nanoparticles and their performance for photocatalytic degradation of 1,2-dichlorethane, Appl. Surf. Sci. 255 (2008) 2205–2213.
[69] L. Shi, D. Weng, Highly active mixed-phase TiO_2 photocatalysts fabricated at low temperature and the correlation between phase composition and photocatalytic activity, J. Environ. Sci. 20 (2008) 1263–1267.
[70] F. Huang, M. Zhou, Y.B. Cheng, R.A. Caruso, Al containing porous titanium dioxide networks: sol–gel synthesis within agarose gel template and photocatalytic activity, Chem. Mater. 18 (2006) 5835–5839.
[71] N. Balász, K. Mogyorósi, D.F. Srankó, A. Pallagi, T. Alapi, A. Oszkó, A. Dombi, P. Sipos, The effect of particle shape on the activity of nanocrystalline TiO_2 photocatalyst in phenol decomposition, Appl. Catal. B: Environ. 84 (2008) 356–362.